# Identifying Myocardial Mechanical Properties from MRI Using an Orthotropic Constitutive Model

Zhinuo J. Wang[1(✉)], Vicky Y. Wang[1], Sue-Mun Huang[1], Justyna A. Niestrawska[2], Alistair A. Young[1,3], and Martyn P. Nash[1,4]

[1] Auckland Bioengineering Institute, University of Auckland, Auckland, New Zealand
{zwan145,shua078}@aucklanduni.ac.nz,
{vicky.wang,a.young,martyn.nash}@auckland.ac.nz
[2] Institute of Biomechanics, Graz University of Technology, Graz, Austria
niestrawska@tugraz.at
[3] Department of Anatomy with Radiology, University of Auckland, Auckland, New Zealand
[4] Department of Engineering Science, University of Auckland, Auckland, New Zealand

**Abstract.** This paper presents a method to characterise the passive orthotropic and contractile properties of left ventricular (LV) myocardial tissue using MRI data of cardiac anatomy, structure and function. Personalised anatomical LV models were fitted to image data from four canine hearts. Diffusion tensor MRI data from the same hearts were parameterised using finite element fitting to provide fibre angle fields that represent longitudinal axes of the myocytes. Fitted fibre angle fields were combined with laminar-sheet orientation data extracted from the Auckland dog heart model and embedded into the customised LV anatomical models. A modified Holzapfel-Ogden orthotropic constitutive relation was parameterised using published data from *ex vivo* shear tests on myocardial tissue blocks. This parameterised constitutive model was scaled for each case in the present study by fitting the individualised LV models to end-diastolic image data. Contractile tension was then estimated by comparing LV model predictions to the end-systolic image data. Personalised models of this kind can be used to predict the 3D deformation and regional stress distributions throughout the LV wall during the entire cardiac cycle.

**Keywords:** Myocardial mechanical properties · Orthotropic constitutive model · Parameter estimation · Canine heart · Passive stiffness · Active contraction · Cardiac cycle

## 1 Introduction

The physiological function of the heart is determined by the mechanical properties of the myocardial tissue. Abnormalities in the mechanical function of the


O. Camara et al. (Eds.): STACOM 2014, LNCS 8896, pp. 135–144, 2015.
DOI: 10.1007/978-3-319-14678-2_14

heart affects its ability to pump blood through the circulatory system, which can lead to fatal consequences. Estimating the mechanical properties of the *in vivo* heart through the use of image-extracted geometries and biophysical modelling provides important information about the stresses and strains that occur during the cardiac cycle. This biomechanical analysis depends on the choice of constitutive model to describe the mechanical properties of myocardial tissue. Many studies have used transversely isotropic constitutive models, for which the fibre and cross-fibre directions can reproduce distinctly different mechanical responses [5]. However, experimental studies have reported that myocardial tissue is not only characterised by the myocardial fibre axis, but also by a distinct laminar organisation, where the tethering between the myocardial cells within a sheet is stiffer than that between adjacent sheets [5]. This motivates the use of orthotropic constitutive models to describe the three distinct axes of microstructural symmetry inherent within the myocardium.

This paper presents a modified version of the Holzapfel-Ogden orthotropic constitutive model [3] for modelling the passive mechanical response of the canine LV. The data used in this paper were provided as part of the MICCAI-STACOM 2014 LV mechanics challenge, which involved comparing model predicted LV displacements with those measured using tagged magnetic resonance imaging (MRI) techniques. The methods presented in this paper have the capability of predicting regional distribution of strain and stress of the LV at both the end-diastolic (ED) and end-systolic (ES) stages of the cardiac cycle.

## 2 Methods

### 2.1 LV Mechanics Modelling

**Anatomical Model Customisation.** Regular truncated prolate spheroid shaped 16 (4 x 4 x 1) element tricubic Hermite finite element (FE) models were fitted to the diastasis canine LV image-derived surface data of each of four cases. For each case, a generic model was first registered to the cardiac coordinate system of the experimental surface data, and then the endocardial and epicardial surfaces were fitted to the data using previously published methods [7].

In order to describe the orthotropic mechanical response of the myocardium, it was necessary to embed fibre and sheet angles into the LV model. Microstructural orientations were described using Euler angles with respect to the short-axis and epicardial tangent planes. Fibre angles were calculated as the helix angles between the projections of the supplied diffusion tensor imaging (DTI) vector data onto the wall tangent plane, and the circumferential axis. Imbrication angles were quantified as the transverse angles that the DTI vectors made with the wall tangent plane, and were found to be sufficiently small to be negligible in this study.

Subject-specific laminar sheet orientation data were not available for the canine hearts in this study, therefore sheet angle data from the Auckland dog heart (ADH) model [5] were incorporated into each of the models. Firstly, each canine LV model was transformed to match the geometry defined by the ADH

model. Then fibre and sheet angle data, extracted directly from the ADH model, were fitted using tricubic Hermite interpolation into each transformed canine model. Since both sets of angles were defined with respect to the local FE material coordinates, the microstructural orientation fields could be directly mapped from the ADH geometry to the new canine models. The embedded sheet angles were adjusted to align the sheet-normal material axes between the DTI and ADH fields in order to produce the best match with the sheet planes described by the ADH model.

For comparative purposes, another set of models were generated based on ADH fibre and ADH sheet data. Predictions using these models were compared to those of the DTI fibre fitted models. The primary difference between the two sets of models was that the ADH data had a broader transmural distribution of fibre angles compared to the DTI-derived models as illustrated in Fig. 1 (see [8] for a detailed comparison).

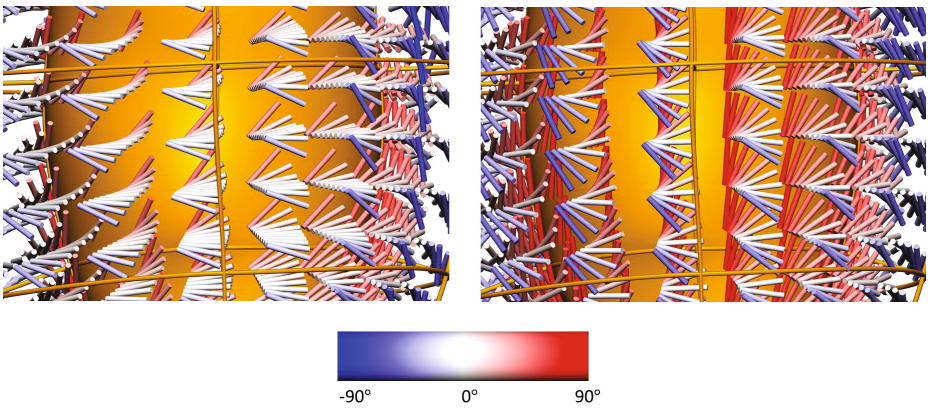


**Fig. 1.** Transmural variation in fibre angles for a mid-posterior portion of the LV model for case A. Left: DTI fitted fibre field. Right: ADH fitted fibre field.

**Myocardial Mechanical Properties.** The passive mechanical response of the myocardium was modelled using a modified version of the Holzapfel-Ogden orthotropic constitutive model [3]. The isotropic (first) term in the original formulation did not allow the mechanical response in each of the material directions to be independently controlled. To decouple the axial terms, the isotropic term was omitted from the original formulation and an additional exponential term describing the sheet-normal direction response was added [2]. The modified formulation is given by

$$W = \sum_{i=\mathrm{f,s,n}} \frac{a_i}{2b_i} \left( \mathrm{e}^{b_i (I_{4i}-1)^2} - 1 \right) + \frac{a_{\mathrm{fs}}}{2b_{\mathrm{fs}}} \left( \mathrm{e}^{b_{\mathrm{fs}} I_{8\mathrm{fs}}^2} - 1 \right) \tag{1}$$

$$\text{where } I_{4\text{f}} = \mathbf{f}_0 \cdot (\mathbf{C}\mathbf{f}_0), I_{4\text{s}} = \mathbf{s}_0 \cdot (\mathbf{C}\mathbf{s}_0), I_{4\text{n}} = \mathbf{n}_0 \cdot (\mathbf{C}\mathbf{n}_0), I_{8\text{fs}} = \mathbf{f}_0 \cdot (\mathbf{C}\mathbf{s}_0) \quad (2)$$

$$\text{and } \mathbf{f}_0 = [1\,0\,0]^T, \mathbf{s}_0 = [0\,1\,0]^T, \mathbf{n}_0 = [0\,0\,1]^T \quad (3)$$

where $\mathbf{C}$ is the right Cauchy-Green deformation tensor referred to the fibre (f), sheet (s) and sheet-normal (n) microstructural material axes, and $a_{\text{f}}$, $a_{\text{s}}$, $a_{\text{n}}$, $a_{\text{fs}}$, $b_{\text{f}}$, $b_{\text{s}}$, $b_{\text{n}}$, $b_{\text{fs}}$ are the constitutive parameters. In keeping with the original Holzapfel-Odgen model, the axial exponential terms only contribute to the strain energy function when their associated invariants $I_{4\text{f}}$, $I_{4\text{s}}$ and $I_{4\text{n}}$ are larger than 1.

The contractile mechanical response of the myocardium was modelled using the steady-state Hunter-McCulloch-ter Keurs active tension constitutive model [4], which is given by

$$T_{\text{a}} = T_{\text{Ca}} \times [1 + \beta(\sqrt{I_{4\text{f}}} - 1)] \quad (4)$$

where $T_{\text{a}}$ is the active tension produced within the tissue, $T_{\text{Ca}}$ is the contractile stress associated with calcium release from the sarcoplasmic reticulum at resting sarcomere length, $\beta$ is the myocardial length-dependence parameter, and $\sqrt{I_{4\text{f}}}$ quantifies the fibre extension ratio.

**LV Mechanics Simulations** were performed for the diastolic slow filling phase (from diastasis to end-diastole) by applying the given LV cavity pressures on the endocardial surfaces of the LV models, while the LV base was constrained to match the motion of the basal epicardial surface data. Diastasis was assumed to be the stress-free reference geometry. Systolic contraction was simulated by increasing the active tension and endocardial pressure loads until the end-systolic values were reached.

### 2.2 Constitutive Parameter Estimation

**Objective Function.** Constitutive parameters were estimated by minimising the mean squared error (MSE) of the projections of the MRI-derived surface data points onto the endocardial and epicardial surfaces of the predicted model.

It was noted that there were discrepancies between the basal motion of the provided surface data and the supplied basal boundary constraints which had been derived from the tagging data. For the purposes of parameter estimation, which was designed to match the supplied surface data, the motion of the base of the LV models was constrained to match that of the surface data so as to exclude this discrepancy from the MSE calculation.

Even though the basal motion was taken from the surface data, following the FE simulations, it was observed that a rotational motion of the model gave a poor match to the surface data for the majority of the ventricle, apart from near the base. To address this problem, the LV models were rigidly aligned with the surface data prior to the computation of the surface projections at each stage in

the parameter estimation process. This method allowed an unbiased comparison of the overall geometry between the model predictions and the surface data, which was independent of the questionable reliability of the prescribed basal motion.

**Parameter Estimation.** Passive parameters were estimated for each of the four cases. The parameters of the passive constitutive model have previously been fitted to simple shear experimental data [1] through a multivariate optimisation process for all six modes of shear. Details of this method can be found in [2]. The fitted values are listed in the Table 1.

**Table 1.** Orthotropic material parameters obtained by fitting to simple shear data [1]

| $a_\mathrm{f}$ (kPa) | $a_\mathrm{s}$ (kPa) | $a_\mathrm{n}$ (kPa) | $a_\mathrm{fs}$ (kPa) | $b_\mathrm{f}$ | $b_\mathrm{s}$ | $b_\mathrm{n}$ | $b_\mathrm{fs}$ |
|---|---|---|---|---|---|---|---|
| 24.84 | 6.94 | 6.35 | 0.37 | 11.32 | 7.07 | 0.22 | 11.67 |

For the purposes of the passive parameter estimation in this study, just two parameters were fitted due to the limited information provided by the diastolic deformation data. With reference to Eq. 5, one parameter ($M_\mathrm{f}$) was used to scale the term associated with the stiffness in the fibre direction, while the second parameter ($M$) was used to scale the remaining terms in the constitutive equation. The rationale behind this model simplification lay in the fact that the LV surface data available for constitutive model parameterisation were only provided at two time points in the cardiac cycle (i.e. ED and ES), which would not contain sufficient kinematic information to estimate all eight passive parameters. Two scaling parameters were estimated instead of just one bulk scaling parameter because analyses showed that there was a substantial improvement in the fit to the ED surface data (data not shown).

$$\begin{aligned} W =& M_f \left( \frac{a_f}{2b_f} \left( \mathrm{e}^{b_f (I_{4f}-1)^2} - 1 \right) \right) \\ &+ M \left( \sum_{i=\mathrm{s,n}} \frac{a_i}{2b_i} \left( \mathrm{e}^{b_i (I_{4i}-1)^2} - 1 \right) + \frac{a_\mathrm{fs}}{2b_\mathrm{fs}} \left( \mathrm{e}^{b_\mathrm{fs} I_{8\mathrm{fs}}^2} - 1 \right) \right) \end{aligned} \tag{5}$$

To estimate the contractile parameters for the four cases, the maximum activation level ($T_{\mathrm{Ca}_\mathrm{max}}$) was determined by matching model predictions to the supplied ES surface data. The length-dependency parameter ($\beta$) in the Hunter-McCulloch-ter Keurs model (Eq. 4) was set to 1.45 as previously reported in [4].

**Simultaneous vs. Sequential Parameter Estimation Schemes.** The framework was set up to estimate the passive and active parameters simultaneously

by summing the errors in projecting the supplied ED and ES surface data onto the surfaces of the model predictions for those states. This approach worked well for the LV models embedded with the ADH fibre data, however the simultaneous estimation method failed for models based on the DTI fibre fields because these models predicted significant apex-to-base lengthening during systole (see Fig. 2 and a discussion of this effect in Section 3.2). Therefore, a sequential parameter estimation method was adopted instead for the models with DTI fibre fields.

### 2.3 Challenge Results

The 2014 LV mechanics challenge required the predictions of material point displacements and fibre stress distributions at ED and ES for each of the four canine hearts. The estimated constitutive parameters from Section 2.2 were used in conjunction with basal constraints that were provided as part of the challenge (these constraints had been derived from the MR tagging data). Regional fibre stress distributions were evaluated as part of the mechanical simulations. The displacements and fibre stresses were evaluated for the material point locations at which the DTI fibre field data were provided. Due to minor discrepancies between the geometric location of the DTI fibre field data and the MRI-derived surface data, some of the material points were found to be positioned outside of the fitted models. This was particularly evident near the base of the LV models. These external points (between 527 and 704 out of 9225 material points for each of the four cases) were excluded from the displacement and stress evaluations.

### 2.4 Computational Modelling Tools

The geometric, fibre and sheet orientation data were fitted using a combination of MATLAB and the computational back-end of the Continuum Mechanics, Image analysis, Signal processing and System identification (CMISS) software package (www.cmiss.org). The CellML open-standard (www.cellml.org) was used to describe the constitutive equation. All three-dimensional model visualisations were rendered using CMGUI (www.cmiss.org/cmgui).

## 3 Results

Parameter estimation results are presented for the sets of models fitted with the DTI and the ADH fibre fields.

### 3.1 Parameter Estimation Using the DTI Fibre Field

The models based on the DTI fibre fields predicted significant apex-to-base lengthening during systole, which yielded large MSEs of the projections at ES. This caused the simultaneous estimation method to fail, with the $M$ and $M_{\mathrm{f}}$ parameters reaching the upper bound (10) because the ED projections were outweighed by the much larger ES projections. To address these issues, the passive

and active parameters were estimated sequentially instead of simultaneously. This allowed the passive parameters to be estimated by fitting only the ED model predictions to the ED surface data, eliminating the issues associated with the apex-to-base lengthening of the ES model predictions. The active parameter ($T_{\mathrm{Ca}_{\max}}$) was subsequently estimated while fixing the passive parameters. The estimated passive and active parameters are presented in Tables 2(a) and 2(b), respectively.

For the contraction phase, the observed apex-to-base lengthening of the LV models led to unreliable projections of the surface data near the LV apex. In an attempt to overcome this problem, the projected locations of the surface data points on the model at DS were embedded and tracked throughout the cardiac cycle, so that a point-to-point vector could be constructed at ES from each surface data point to their corresponding tracked location on the model surface. The longitudinal components of these vectors were substituted for the longitudinal components of the untracked surface projections at ES to construct a mixed objective function for fitting these DTI-based models. This mixed objective function was designed to penalise apex-to-base model lengthening while remaining insensitive to model twisting in the short-axis plane. However, the lengthening problem was not eliminated even at the optimal value of $T_{\mathrm{Ca}_{\max}}$ (see Fig. 2), resulting in the large MSE values presented in Table 2(b).

**Table 2.** Passive ($M_{\mathrm{f}}$ and $M$) and active ($T_{\mathrm{Ca}_{\max}}$) parameters estimated for LV models embedded with the DTI fibre field data

| Cases | $M_{\mathrm{f}}$ | $M$ | ED MSE ($\mathrm{mm}^2$) |
|---|---|---|---|
| A | 0.98 | 1.18 | 0.38 |
| B | 0.60 | 1.09 | 0.45 |
| C | 0.70 | 1.23 | 0.37 |
| D | 4.93 | 3.51 | 0.15 |

(a)

| Cases | $T_{\mathrm{Ca}_{\max}}$ (kPa) | ES MSE ($\mathrm{mm}^2$) |
|---|---|---|
| A | 53.8 | 43.9 |
| B | 46.8 | 18.7 |
| C | 31.9 | 26.5 |
| D | 30.1 | 23.8 |

(b)

### 3.2 Parameter Estimation Using the ADH Fibre Field

The results of simultaneously estimating the passive and active constitutive parameters for the LV models based on the ADH fibre data are presented in Table 3. The use of ADH fibre data with optimal constitutive parameters gave rise to substantially smaller surface data projections at ES.

A comparison between the model predictions based on the DTI versus ADH fibre fields (Fig. 2) showed that the apex-to-base lengthening observed for the models based on the DTI fibre fields was reduced for the models based on the ADH fibre field in all four cases.

**Table 3.** Simultaneous estimation of the passive ($M_f$ and $M$) and active ($T_{Ca_{max}}$) parameters for LV models embedded with the ADH fibre field data

| Cases | $M_f$ | $M$ | $T_{Ca_{max}}$ (kPa) | ED MSE ($mm^2$) | ES MSE ($mm^2$) | Total MSE ($mm^2$) |
|---|---|---|---|---|---|---|
| A | 2.30 | 1.77 | 125.1 | 0.46 | 1.31 | 0.89 |
| B | 0.56 | 0.94 | 60.3 | 0.47 | 0.99 | 0.73 |
| C | 0.86 | 1.25 | 46.1 | 0.40 | 1.42 | 0.91 |
| D | 3.07 | 4.48 | 50.4 | 0.13 | 2.62 | 1.38 |

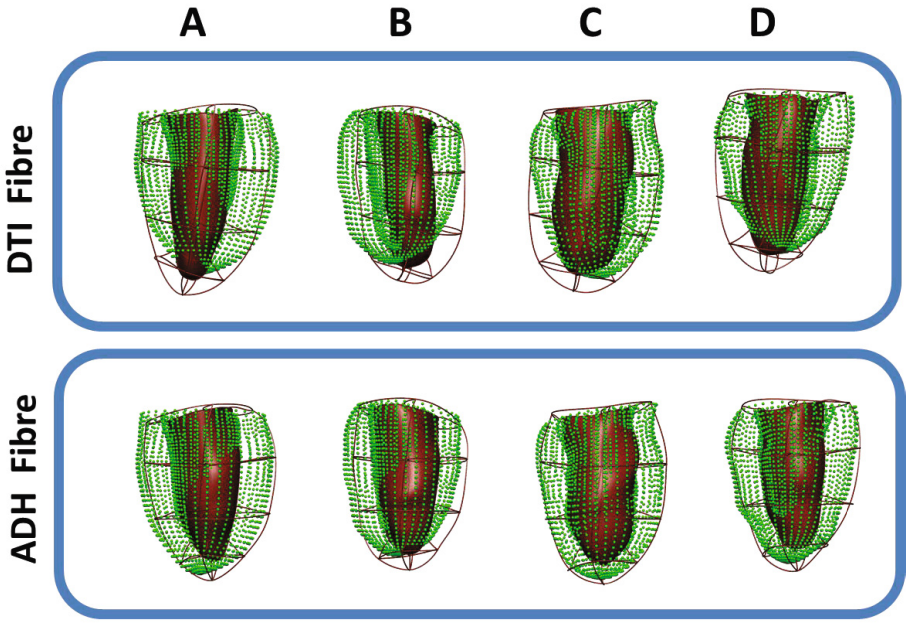


**Fig. 2.** Optimal end-systolic (ES) models for cases A, B, C and D, comparing deformation predictions for LV models based on the DTI fibre field (top panel) against those based on the ADH fibre field (bottom panel). The endocardium (brown surfaces) and epicardium (brown lines) of the predicted LV models are superimposed with the supplied surface data (green points) for the ES state.

### 3.3 Regional Strain and Stress Distributions

The individualised FE models were used to predict the strain and stress distributions throughout the ventricular walls during the cardiac cycle. An example of the stress distribution evaluated for case A is shown in Fig. 3.

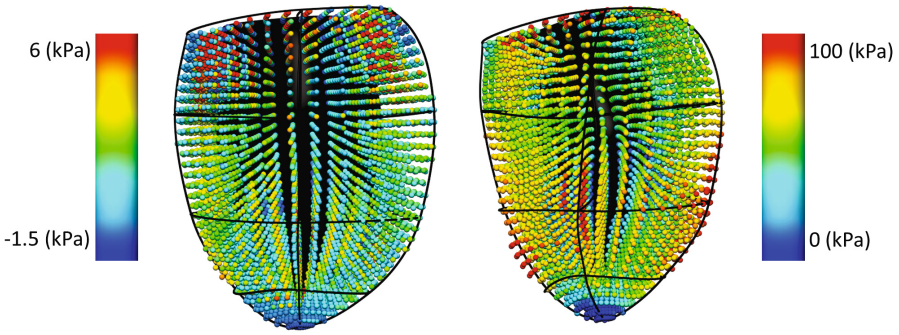


**Fig. 3.** Total Cauchy fibre stress distribution using the ADH fibre field at ED (left) and ES (right)

## 4 Discussion and Conclusions

In this study, an orthotropic passive constitutive model and an active tension model were parameterised using MRI-derived surface data. The objective function was the MSE of the projections from the MRI-derived data to the surfaces of the predicted LV models.

Sets of models were constructed using DTI-derived fibre fields, and the ADH fibre field. The major point of difference between the predictions for the two sets of models was that the LV long axis dimension of the ADH fibre field models did not lengthen as much as the DTI fibre field models during systolic contraction. The mechanism for this difference is most likely to be related to the differences in the transmural ranges of fibre orientations between the two sets of models, which have been quantified in [8].

Even though the constitutive model was orthotropic, just two passive parameters could be estimated due to insufficient information contained within the supplied surface data, which did not track myocardial material points, but instead simply characterised the LV surface shapes. The parameter estimation process was constrained such that the stiffness in the fibre direction was able to vary independently to the stiffness for the other components of the constitutive equation. It would be interesting to explore further the performance of a transversely isotropic constitutive model in biomechanical analysis and parameter estimation using these data.

A simultaneous passive and active parameter estimation method was performed for the models fitted with the ADH fibre field. The inclusion of ES error projections in the estimation of passive parameters allowed them to be tuned using a larger range of deformations. This was particularly important when the diastolic deformations were very small, as observed in case D in this study, which made it difficult to identify the optimal passive parameters using just the ED data. Simultaneous parameter estimation failed for the DTI fibre field fitted models because the predicted elongation caused the large ES projection errors

to markedly outweigh the ED projection errors in the objective function. This sent the passive parameters to their upper bounds during the estimation process. When LV models based on the ADH fibre fields were used for parameter estimation, the objective function was more balanced in terms of the contributions of the ED and ES projection errors. In consequence, the parameter estimation procedure was much more stable compared to that of the DTI fibre models. A limitation of the simultaneous estimation method was that correlation was found between the $M_{\mathrm{f}}$ and $M$ parameters as well as between the $M$ and $T_{\mathrm{Ca}_{\mathrm{max}}}$ parameters. These correlations should be investigated further.

The model predicted regional distributions of fibre stress could provide insights into the mechanical behaviour of the myocardium that are not derivable from cardiac imaging techniques. These stress distributions could also be useful for investigating the myocardial work performed across different regions of the LV wall during the cardiac cycle.

## References

1. Dokos, S., Smaill, B.H., Young, A.A., LeGrice, I.J.: Shear properties of passive ventricular myocardium. American Journal of Physiology **283**, H2650–H2659 (2002)
2. Niestrawska J.: A structure-based analysis of cardiac remodelling - a constitutive modelling approach. Masters Thesis, RWTH Aachen University of Technology, Germany (2013)
3. Holzapfel, G.A., Ogden, R.W.: Constitutive modelling of passive myocardium: a structurally based framework for material characterisation. Philosophical Transactions of the Royal Society A **367**(1902), 3445–3475 (2009)
4. Hunter, P.J., McCulloch, A.D., Ter Keurs, H.E.D.J.: Modelling the mechanical properties of cardiac muscle. Progress in Biophysics and Molecular Biology **69**(2–3), 289–331 (1998)
5. LeGrice, I.J., Hunter, P.J., Smaill, B.H.: Laminar structure of the heart: a mathematical model. American Journal of Physiology **272**, H2466–H2476 (1997)
6. Nielsen, P.M.F., LeGrice, I.J., Smaill, B.H., Hunter, P.J.: Mathematical model of geometry and fibrous structure of the heart. American Journal of Physiology **260**(4), H1365–H1378 (1991)
7. Wang, V.Y., Lam, H.I., Ennis, D.B., Cowan, B.R., Young, A.A., Nash, M.P.: Modelling passive diastolic mechanics with quantitative MRI of cardiac structure and function. Medical Image Analysis **13**(5), 773–784 (2009)
8. Wang, V.Y.: Modelling in vivo cardiac mechanics usng MRI and FEM. PhD Thesis, Auckland Bioengineering Institute, University of Auckland, New Zealand (2012)